

Deformation and Damage Mechanisms of Zinc Coatings on Hot-Dip Galvanized Steel Sheets: Part II. Damage Modes

RODOLPHE PARISOT, SAMUEL FOREST, ANDRÉ PINEAU, FRANCK NGUYEN,
XAVIER DEMONET, and JEAN-MICHEL MATAIGNE

Zinc-based coatings are widely used for protection against corrosion of steel-sheet products in the automotive industry. The objective of the present article is to investigate the damage modes at work in three different microstructures of a zinc coating on an interstitial-free steel substrate under tension, plane-strain tension, and expansion loading. Plastic-deformation mechanisms are addressed in the companion article. Two main fracture mechanisms, namely, intergranular cracking and transgranular cleavage fracture, were identified in an untempered cold-rolled coating, a tempered cold-rolled coating, and a recrystallized coating. No fracture at the interface between the steel and zinc coating was observed that could lead to spalling, in the studied zinc alloy. A complex network of cleavage cracks and their interaction with deformation twinning is shown to develop in the material. An extensive quantitative analysis based on systematic image analysis provides the number and cumulative length of cleavage cracks at different strain levels for the three investigated microstructures and three loading conditions. Grain refinement by recrystallization is shown to lead to an improved cracking resistance of the coating. A model for crystallographic cleavage combining the stress component normal to the basal plane and the amount of plastic slip on the basal slip systems is proposed and identified from equibiaxial tension tests and electron backscattered diffraction (EBSD) analysis of the cracked grains. This analysis requires the computation of the nonlinear stress-strain response of each grain using a crystal-plasticity constitutive model. The model is then applied successfully to other loading conditions and is shown to account for the preferred orientations of damaged grains observed in the case of plane-strain tension.

I. INTRODUCTION

ZINC coatings on steel substrates for applications in the automotive industry are subjected to severe loading conditions during stamping processes. This can result in the damage of the coating and, eventually, degradation of the surface aspect or pollution of the forming tools. It is important to determine which damage mechanisms like intergranular, cleavage, or interface cracking are responsible for coating spalling.

Much attention has been paid in the literature to the characterization of damage processes at work in zinc coatings of various types: electrodeposited and hot-dip galvanized steel sheets.^[1] The authors usually try to relate metallurgical data like texture, grain size, or chemical segregation to damage appearing at large strain levels. For instance, in Reference 2, the authors show that intergranular cracks can be present in the coating of a hot-dip galvanized steel sheet prior to any deformation. These cracks are supposed to be formed during the cooling process after deposition, due to the difference between the thermal-expansion coefficients of zinc and the steel substrate. They open when the coated sheet is strained. Transgranular cracks are observed at larger strains in some grains. These are supposed to be cleavage cracks that appear

in grains in which no deformation twinning has previously occurred. The crystallographic texture effect on the deformation and damage modes of zinc coatings was investigated in Reference 3. In particular, it is shown that grains having their *c*-axis perpendicular to the sheet plane (called basal grains in the following text) are prone to deformation twinning. This deformation mode is accompanied by a rotation of about 90 deg of the *c*-axis in the twinned crystal with respect to the parent crystal.^[4] As a result, the twins originally in the basal grains become favorably oriented for cleavage when tensile stress is applied along a direction in the sheet plane. Twins are not observed in the bulk zinc material studied in Reference 5, nor in small-grained pure zinc.^[6]

Grain size also has an effect on the damage mechanisms in zinc coatings, as shown in Reference 7. These authors compare the mechanical behavior of two different zinc coatings for the same steel substrate: the first one is made of flat “pancake” zinc grains with an in-plane size 20 times greater than the thickness of the coating (about 8 μm). The second coating has been brushed, leading to partial recrystallization of the coating. The new grain diameter is about 30 μm . When subjected to two different mechanical tests (tension test up to 25 pct and folding test at 180 deg), the first zinc coating is more damaged than the second one. Intergranular cracking is found to be the leading mechanism in tension, whereas cleavage cracks are more numerous after the folding test. Twins are found only in the first coating. The analyses proposed in the previous articles remain, however, purely descriptive.

The aim of the present work is to provide a quantitative analysis of damage mechanisms at work in an alloyed zinc coating and to derive a local cleavage criterion working under uni- and multiaxial loading conditions. Three different microstructures of the same material are considered: an

RODOLPHE PARISOT, formerly Ph. D. student, now Maintenance Project Manager, with the Centre des Matériaux, Ecole des Mines de Paris/CNRS, BP 87, 91003-Evry, France, is Director of Maintenance, Air France, 95074 Roissy CDG, France. SAMUEL FOREST, Researcher, ANDRÉ PINEAU, Professor, and FRANÇOIS GRILLON, Researcher, are with the Centre des Matériaux, Ecole des Mines de Paris/CNRS. Contact e-mail: samuel.forest@ensmp.fr XAVIER DEMONET, Research Engineer, and JEAN-MICHEL MATAIGNE, Research Director, are with CED, ARCELOR Recherche et Développement, BP 39109, 60761 Montataire, France.

Manuscript submitted April 8, 2003.

untempered cold-rolled coating, a tempered cold-rolled coating, and a recrystallized coating. They all have the same thickness of $8\ \mu\text{m}$. The deformation modes of these three different microstructures are presented in detail in Part I of this article,^[5] where they are compared to the deformation mechanisms found in a reference bulk zinc alloy. The development of damage modes is traced from the early stage of plasticity to about a 10 pct equivalent strain. Three loading conditions are considered for the coated steel substrate, as in Reference 5: tension, plane-strain tests, and equibiaxial expansion.

Two main damage modes have been observed and quantified: intergranular cracking and cleavage cracking. They are shown to be stress-relaxing mechanisms that prevent the coating from spalling, as already observed by Focht.^[8] In particular, in the case of the specific alloyed zinc coating investigated in this work, no fracture at the interface between the steel and zinc has been observed, even after more than a 15 pct equivalent strain. This is due to the exceptional strength of an intermetallic Fe_2Al_5 ultrathin layer at the interface. The role of this layer for spalling prevention is not addressed in the present work. The reader is referred to Reference 9 for a metallurgical description of this intermetallic layer and to Reference 10 for its role in stress-corrosion cracking of hot-dip galvanized steel sheets. An important feature of the damage processes is the competition between deformation twinning and cleavage inside the grains.

The three microstructures of the investigated zinc coating, as well as the steel substrate, are presented in Reference 5. The main features are recalled in Section II. Zinc has a hexagonal crystallographic structure with a ratio of $c/a = 1.856$. The cleavage plane is the basal plane (0001).^[11] Other crystallographic concepts, including labeling and representation of slip and twinning systems, are given in Part I of this article.^[5] Mechanical testing, microstructural observation, and image-analysis methods are presented in Section II. Results follow in Section III: identification and a detailed description of the damage modes, depending on the grain size and presence or lack of an oxide layer. A quantitative analysis of the number of cleavage cracks as a function of loading conditions at different strain levels is proposed using systematic image analysis. In Section IV, the cleavage criterion initially proposed by Gilman^[11] is slightly extended. Its parameters are identified from the previous quantitative and crystallographic information. The identification requires the estimation of the stress state in each grain. This is done using the simple relaxed-constraint Taylor-like model introduced and validated in Part I of this article.^[5] The model can then be applied to the three different loading conditions.

II. EXPERIMENTAL PROCEDURES AND IMAGE ANALYSIS TECHNIQUE

A. Materials

The 0.7-mm-thick substrate of the investigated coating is an interstitial-free steel, the chemical composition of which is given in Table II of Part I of this article.^[5] The grain size of the substrate is $d = 10\ \mu\text{m}$. The zinc deposition process leads to a coating made of very flat zinc grains, with only one grain through the thickness. Full details on material processing are given in Reference 5. The damage modes are investigated for the three following microstructures of the alloyed zinc coating.

1. *untempered cold-rolled coating*, labeled “NSK”. It is obtained after stopping the industrial process just after the solidification of zinc grains.
2. *tempered cold-rolled coating*, labeled “SK”. The industrial hot-dip galvanized steel sheets undergo tempered rolling (a slight rolling of about 1.3 pct) just after they emerge from the galvanizing bath.^[12] This induces the formation of many twins due to the compressive stresses induced by rolling.
3. *recrystallized coating*, labelled “recrystallized” or “R”. This condition is obtained after a recrystallization heat treatment applied to the SK coating. The resulting in-plane grain size is about $30\ \mu\text{m}$, with still one single grain through the thickness.

The NSK and the SK coatings exhibit a pancake grain with in-plane sizes ranging from 200 to $600\ \mu\text{m}$ and only one grain through the thickness of the coating ($d = 8\ \mu\text{m}$). More details concerning the deformation modes and metallographic observations of these three microstructures are given in Part I of this article.^[5] In particular, basal slip (three systems) is the easiest deformation mode, followed by pyramidal π_2 slip (six systems), prismatic slip (three systems), pyramidal π_1 slip (six systems), and deformation twinning (six systems). The critical resolved shear stress for basal slip is at least 5 to 10 times smaller than that for the other deformation modes. However, it has been shown that pancake grains of the NSK and SK coatings display at least three deformation modes and deform mainly by pyramidal π_2 slip and twinning. This has been proven to be due to the combined texture of the zinc coating and to substrate effects.^[5]

B. Mechanical Testing Methods

The following mechanical tests were performed at room temperature: tensile tests, plane-strain tests on $45 \times 65 \times 0.7\ \text{mm}$ specimens, and equibiaxial expansion tests on $65 \times 65 \times 0.7\ \text{mm}$ specimens. The rolling direction (RD), transverse direction (TD), and normal direction (ND) are denoted by (1, 2, 3) \equiv (RD, TD, ND) in the following text. Tension tests (in the RD only, in the present article) were performed on a Zwick (Ulm, Germany) machine using a 5 kN cell. The gage length and width of the tensile specimens were 75 and 12.5 mm, respectively, for the NSK and SK materials. Both plane-strain tests ($\epsilon_{11} > 0$ and $\epsilon_{22} \approx 0$) and equibiaxial expansion tests ($\epsilon_{11} = \epsilon_{22} > 0$) are performed on an Erichsen (Horner, Germany) stamping machine. Strains were measured after the test, looking at the deformation of a network of 3-mm-diameter circles deposited before the test. The strain rate was $\dot{\epsilon} = 10^{-4}\ \text{s}^{-1}$ for the tension, plane-strain, and expansion tests. Equivalent strain is defined in this work as

$$\epsilon_{eq} = \sqrt{\frac{2}{3} \epsilon_{ij} \epsilon_{ij}} \quad [1]$$

where repeated indices must be summed up.

In all micrographs shown in this article, the tensile loading axis is horizontal, if not otherwise stated.

C. EBSD Analysis

Global and local crystallographic texture analyses have been performed. The global textures are provided in Section III-C

of Part I of this article for the three microstructures NSK, SK, and R. Strongly basal textures have been found, with the c -axis of most grains almost normal to the sheet plane (figures 6(a) through (c) of the companion article).

In the present work, the EBSD technique is used systematically to determine the local lattice orientation of the grains displaying cleavage cracks after straining, for the three different loading conditions. In particular, it has been observed that these cracks coincide with the trace of the (0001) plane. Details on the specific EBSD technique used are given in Part I of this article.^[5]

In addition, the EBSD technique is used also to identify the relative orientations of twins and parent crystals in individual grains. The analysis of the corresponding rotation makes it possible to identify the twinning system. In particular, twins appearing at the tip of cleavage cracks have been identified by means of the EBSD technique.

D. Image-Analysis Technique for Cracks

Two different types of cracks are observed after straining: intergranular cracks, on the one hand, and intragranular cleavage cracks, on the other hand. A quantitative analysis of cleavage-crack number and length has been performed based on systematic image analysis.

Individual cracks are identified and labeled in several grains after mechanical testing at a given equivalent strain level. The main difficulty lies in the discrimination of cleavage cracks from intergranular cracks. Figure 1 shows that intergranular cracks are significantly more wavy than cleavage cracks. The sinuous character of each identified crack branch is quantified by the linear-correlation index of its approximation by a straight line. The choice of a suitable threshold makes it possible to distinguish cleavage cracks from intergranular ones. This criterion depends, in fact, on crack length:

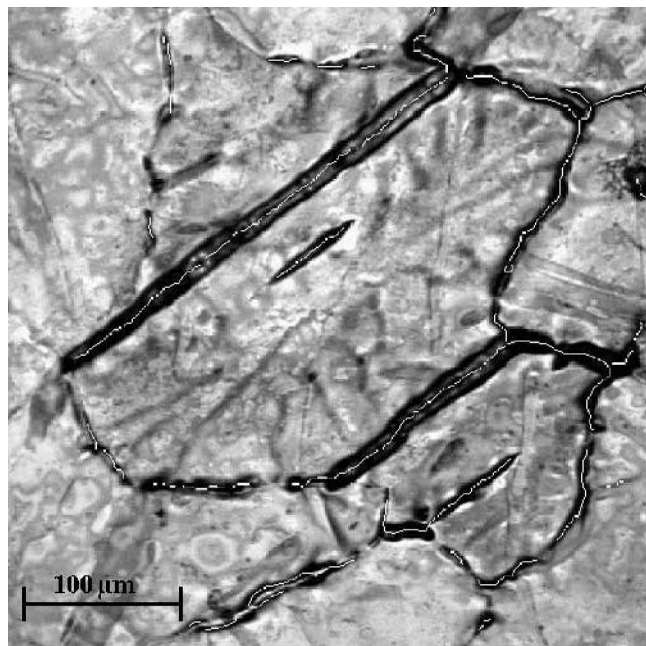


Fig. 1—Distinction between wavy intergranular cracks I and rectilinear cleavage cracks C by image analysis: four cleavage cracks with two of them connecting intergranular cracks.

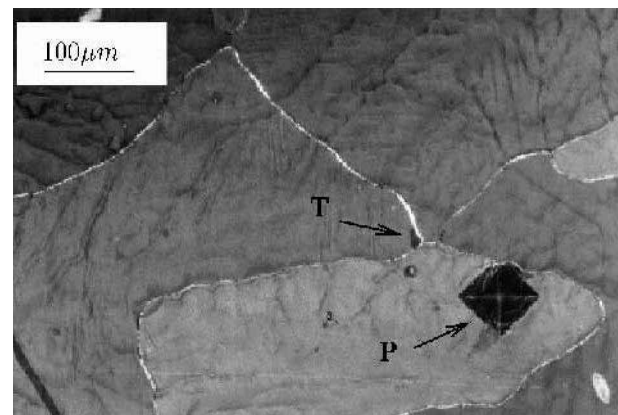
for longer cracks, the threshold for correlation indices is closer to 1. If the crack is wavy, it is divided into subcracks, and the previous analysis is carried out again for each subcrack. This procedure is necessary when a straight crack (*i.e.*, a cleavage crack) joins a sinuous cracked grain boundary like in Figure 1. The straight part of the crack can be separated from its sinuous part. The resulting data consist of a list of individual crack lengths. The number and cumulative length of cracks on a given surface of the coating can be deduced.

These operations are repeated at different strain levels on different specimens for each loading condition.

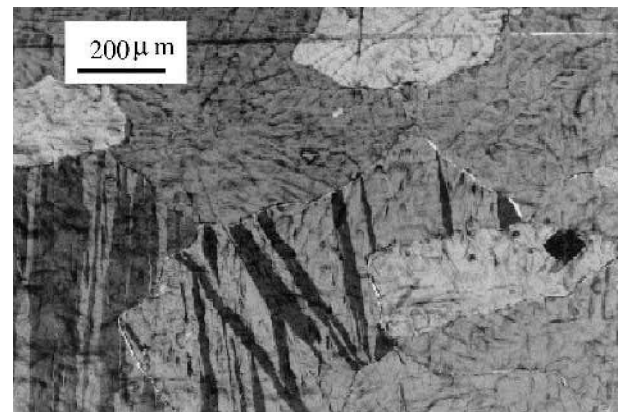
III. RESULTS

A. Intergranular Cracking

Grain boundaries are visible on undeformed samples due to thermal grooving effects associated with the solidification process. After deformation, the opening of many grain boundaries is observed very early in tensile deformation of all the coatings. Such intergranular cracks can be seen in Figure 2(a). Further observations are needed to assess the severity of such cracks regarding possible subsequent spalling



(a)



(b)

Fig. 2—Nucleation and growth of a twin in a grain exhibiting intergranular cracking (NSK coating, tensile test). (a) The twin nucleus T can be seen as a black spot at the triple junction near the indentation point P at $\epsilon_{eq} = 7.5$ pct. (b) At $\epsilon_{eq} = 15$ pct, the twin has grown in spite of the broken neighboring grain boundaries.

processes. The two following observations indicate that, far from being the precursor of zinc grain damage, intergranular cracks simply alleviate stress concentrations associated with the incompatibility of plastic deformation near grain boundaries.

Figures 2(a) and (b) were taken at two different increasing tensile strain levels. A very small twin can be seen to nucleate at a grain corner close to an indentation point in Figure 2(a). In spite of the apparent opening of the neighboring grain boundaries, this twin can be shown to grow further after subsequent straining in Figure 2(b), where other twins have formed inside the central and neighboring grains. This suggests that the investigated zinc grain is still able to sustain the deformation carried by the substrate and, therefore, that the substrate/coating interface is not damaged even close to cracked grain boundaries.

Another indication for that is provided by Figure 3. It shows two areas of a NSK specimen tested in equibiaxial expansion. On the left-hand side, lacquer was applied after the test, whereas the right-hand side was electropolished. It can be seen that the decohesion that is clear on the left-hand side almost disappears on the right-hand side. The intergranular decohesion does not seem to reach the substrate/coating interface. Accordingly, the interface is not exposed to the ambient atmosphere.

As a result, intergranular cracks are not believed to be responsible for further damage of zinc grains, nor possible spalling. That is why the intergranular cracking process is not studied in more detail in this work.

In contrast, Figure 4 shows a cleavage crack on the same specimen. The naked interface can be seen at some locations. Chemical microanalysis at the bottom of the crack indicates the presence of Zn, Fe, and Al in specific ratios. This suggests that the revealed surface is an intermetallic compound which serves as the interface between the steel and zinc coating.

The aforementioned reasons explain why attention is now focused on intragranular cleavage cracking.

B. Cleavage Cracks

Cleavage is found to be an active damage mechanism only in the case of multiaxial loading. Cleavage cracks are numerous in the case of equibiaxial expansion and absent in simple tension loading. Other qualitative features of cleavage cracks depend on the specific microstructure. They are reported subsequently.

1. NSK coating

The cleavage cracks observed on the NSK coating under equibiaxial expansion cross the entire grain and stop at the grain boundaries. Figures 5 and 6 show the evolution of intragranular damage at four strain levels for an equibiaxial tensile test. The photos have been obtained after chemical etching by optical microscopy under polarized light. The composition of the etching solution was 300 mL ethylic alcohol (C_2H_5OH) + 500 mL phosphoric acid (H_3PO_3). Figure 5(a) shows the typical situation after $\epsilon_{eq} = 5.3$ pct equibiaxial expansion: one white grain and one blue grain are damaged by several parallel cracks that appear brighter than the white grain on the picture. Twins are emitted by the crack (blue twins in the white grain and white twins in the blue

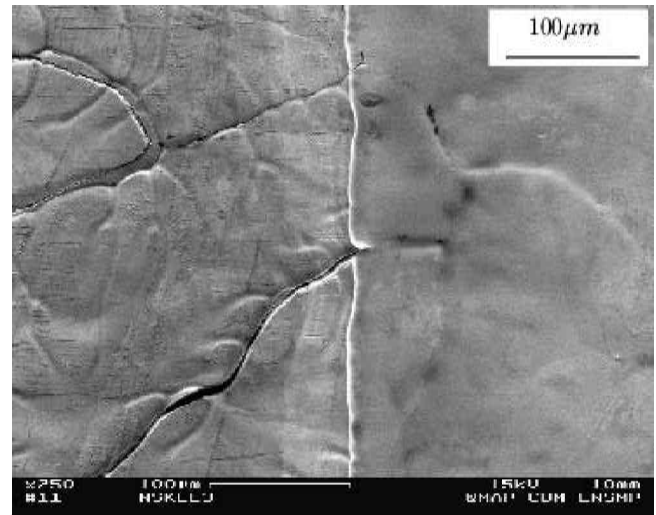


Fig. 3—Intergranular cracking after equibiaxial expansion of NSK coating: the right area is electropolished, whereas the left area is not. It indicates that the cracks do not reach the interface.

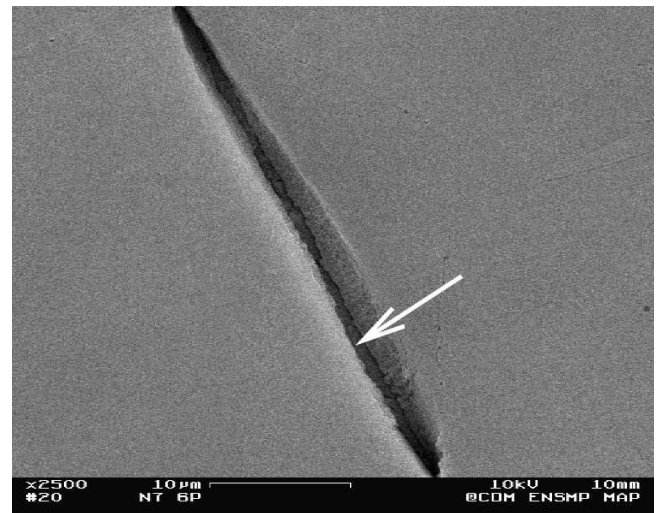
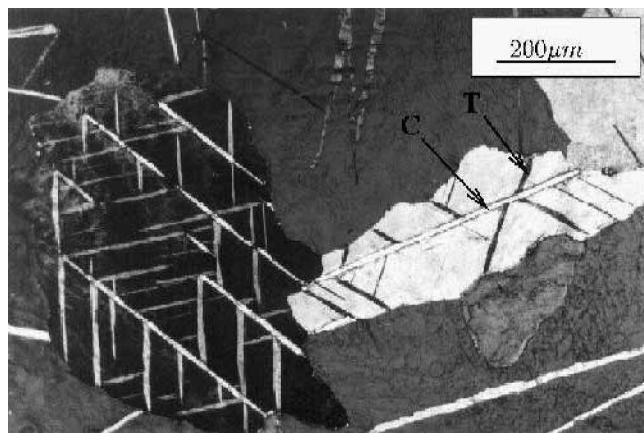


Fig. 4—Cleavage crack on a NSK specimen; the arrow indicates the location of naked substrate/coating interface.

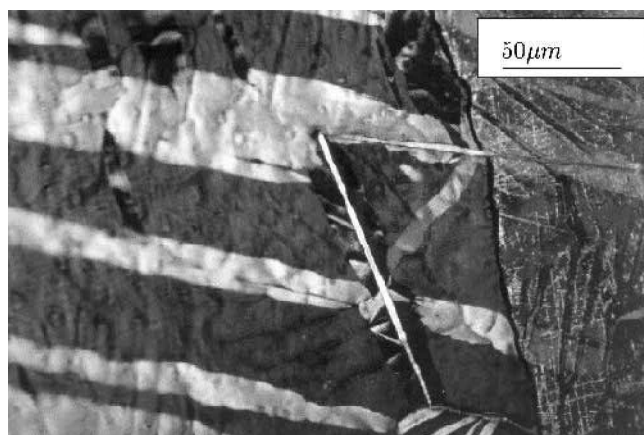
grain) symmetrically with respect to the cleavage crack. This phenomenon has been proposed by Bilby and Bullough^[13] and reported by Yoo^[14] as a possible stress-relaxation mechanism at the crack tip.

Initially, some grains may be adversely oriented for cleavage cracking, so that only networks of twins can be seen inside some grains (Figures 5(b) and 6(a), for instance), in the form of regularly spaced white and blue twins. Some newly appeared twins can then be properly oriented for subsequent cleavage. That is why cleavage cracks are observed inside two twins in Figure 5(b). These cracks emit twins inside a twin.

Further straining is associated with the formation of additional cleavage cracks inside the damaged grains (Figure 6(a)). At larger strains, deformation due to cleavage cracking is accommodated by denser and denser twin



(a)



(b)

Fig. 5—Equibiaxial expansion test on the NSK coating at two different equivalent strain levels: (a) twins (T) along cleavage cracks (C) at $\epsilon_{eq} = 5.3$ pct and (b) cleavage crack within a twin at $\epsilon_{eq} = 11.3$ pct. Polarized light micrographs.

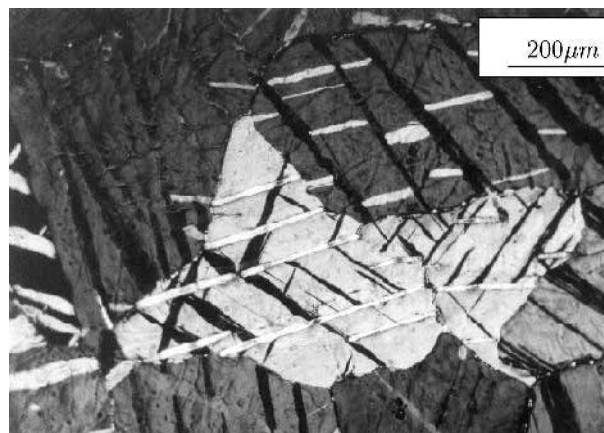
networks (Figure 6(b)). Note the resulting fishbone structure of cleavage cracks and their twins.

2. SK coating

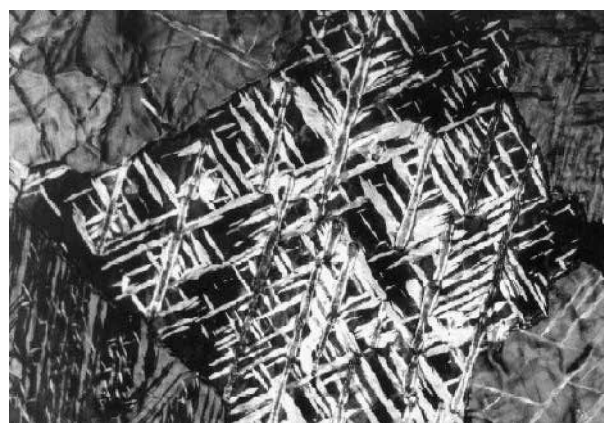
The microstructure has a strong influence on the damage evolution of the coatings. The numerous small twins induced by the tempered rolling in the SK coating are strong obstacles to the development of cleavage cracks. Cleavage cracks are, therefore, about 5 times smaller than in the NSK coating. The lattice misorientation introduced by a twin in front of a propagating cleavage crack is close to 90 deg, so that the crack must stop. Cleavage cracks are stopped by twins and grain boundaries. Even for extreme strain levels of $\epsilon_{eq} = 27$ pct, one does not see more than one cleavage crack per grain.

3. Recrystallized coating

Cleavage cracks found on the fine-grained coating are about as small and as rare as in the SK coating, as can be seen from Figure 7. It has been shown in Reference 5 that mechanical twinning is not a major deformation mode of the recrystallized coating. Therefore, grain boundaries are the only obstacles to cleavage-crack propagation in the small-grained microstructure.



(a)



(b)

Fig. 6—Equibiaxial expansion test on the NSK coating at two different equivalent strain levels: (a) twin network without cracking in the upper right grain and cleavage cracks in the two central grains, at $\epsilon_{eq} = 11.3$ pct. (b) Multiple cleavage cracking after large straining $\epsilon_{eq} = 29$ pct. Polarized light micrographs.

C. Orientation of Cleavage Cracks

In the case of plane-strain tension, the cleavage cracks do have special orientations with respect to the main loading axis. Direct and inverse pole figures for 47 damaged grains identified in the NSK coating are given in Figure 8 after a plane-strain test in the RD direction. It can be seen that the c -axis of most of the cleaved grains is close to the main loading RD, even though cleavage cracks have also been found in other grains far from this ideal orientation (left-hand sides of Figures 8(a) and (b)). Many cleavage cracks are, therefore, normal to the tensile direction. Since the texture of the coating is such that the c -axis of zinc grains is close to the ND, one realizes that cleavage takes place in a small number of grains that do not have this ideal orientation, or in twins.

Interestingly, the secondary orientation of cleaved grains with the c -axis close to the tensile axis is not fully isotropic, as shown by the right-hand sides of Figures 8(a) and (b). The ND is found to be close to the $\langle 10\bar{1}0 \rangle$ direction of the cleaved grains. This cannot be explained solely by the texture of the NSK coating which does not exhibit this feature (Figure 5(a) of Part I of this article^[5]). A reliable cleavage-fracture criterion, as developed in

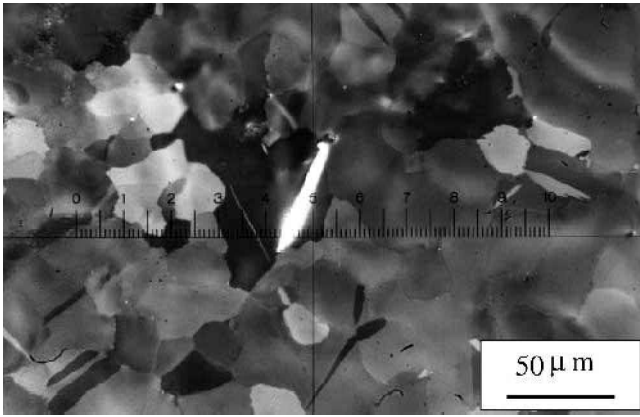


Fig. 7—Equibiaxial expansion test on the recrystallized coating: $\epsilon_{eq} = 25$ pct. The cleavage crack is about 30- μm long.

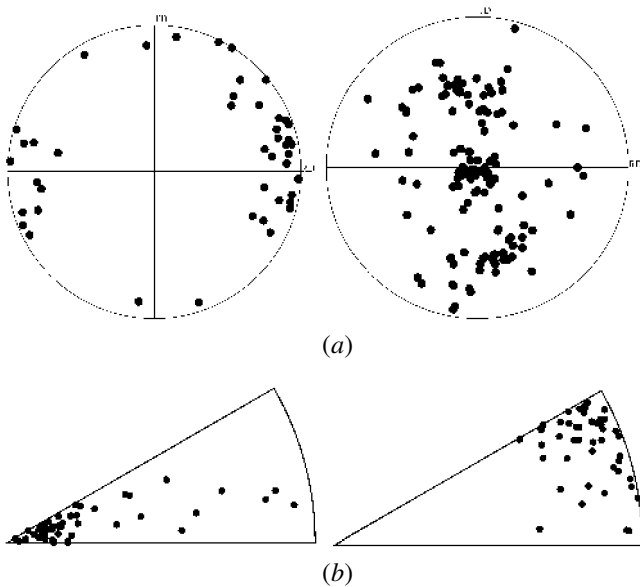


Fig. 8—Pole figures representing cleaved grains in a plane strain test after 10 pct: (a) (0002) pole figure on the left and $\langle 10\bar{1}0 \rangle$ pole figure on the right; and (b) inverse pole figures for the tensile axis RD (left) and for the direction ND (right).

Section IV–A, should be able to account for these crystallographic observations.

D. Crack-Length Distributions and Evolution with Straining

The image-analysis technique described in Section II–D has been applied to determine the number and length of cleavage cracks in the three investigated coatings under plane-strain and equibiaxial expansion and at different equivalent strain levels. For each coating, loading condition, and strain level, one different sample is analyzed. For each sample, a surface of 1 cm^2 is considered. We define the number of individual cleavage cracks on 1 cm^2 , and their cumulative length, *i.e.*, the sum of the individual crack lengths of 1 cm^2 . Another interesting quantity is the mean crack length, computed as the ratio of the cumulative crack length divided by the number of cracks. The results concerning the

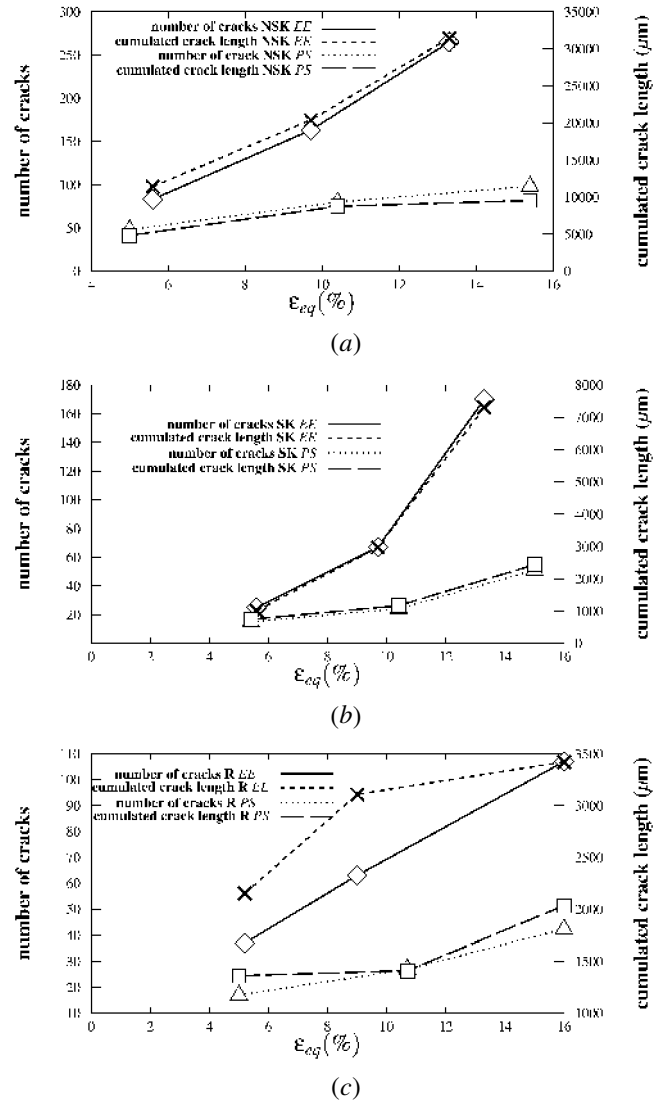


Fig. 9—Number of cracks and cumulative crack length as a function of equivalent strain on a surface of 1 cm^2 : (a) NSK coating, (b) SK coating, and (c) recrystallized (R) coating (*EE* stands for equibiaxial expansion test; *PS* stands for plane strain test).

number of cracks and cumulative crack length are given in Figures 9(a) through (c) for the three different microstructures, respectively, at three equivalent strain levels (about 5, 10, and 15 pct).

The main result is the following: the smaller the grain size, the smaller the mean and cumulative crack length. The mean crack length is found to be $118 \mu\text{m}$ for the NSK coating, $44 \mu\text{m}$ for the SK coating, and only $33 \mu\text{m}$ for the recrystallized coating. The cumulative crack length of the SK coating is 3 to 4 times smaller than that for the NSK coating. The cumulative crack length of the recrystallized coating is even 10 times smaller. This ratio is found to be independent of the strain level. This difference is due to the fact that the stress state is very different for pancake or more-equiaxial grains. The finite-element analysis performed in Reference 15 shows that the stress state in pancake grains is strongly multiaxial due to the deformation prescribed by the substrate to the individual pancake grains. These high-stress states

explain the activation of pyramidal π_2 slip and, eventually, of cleavage. In contrast, the finite-element analysis performed in Part I of this article^[5] for more-equiaxed grains shows that basal slip is the main plasticity mechanism, associated with lower stresses.

As a result, a grain refinement for a given coating thickness is shown here to enhance the damage resistance of zinc coatings on galvanized steel sheets.

E. Oxide-Layer Effect

The oxide layer that is always present on zinc-coated steel sheets can be shown to play an important role in the cleavage fracture of zinc grains. For that purpose, the previous quantitative analysis of cleavage cracking has been carried out again for electropolished specimens of the three different coatings. Electropolishing leads to a thickness reduction of the coating smaller than 1 μm . Figure 10 shows the obtained number and cumulative length of cracks at three different equivalent strain levels. The absence of the oxide layer does not influence the fact that the cumulative crack length is about 3 times smaller for the SK and R coatings than for the NSK coating. The most striking feature is that the number and length of cracks is found to be dramatically reduced when the oxide layer is removed, by a factor of almost 10 for the NSK coating, for instance.

An explanation for that is not yet available. One may argue that the presence of an oxide layer that is incoherent with the zinc coating leads to the formation of dislocation pileups at the zinc/oxide interface. This may result locally in higher stresses promoting the nucleation of cleavage cracks.

IV. DISCUSSION AND MODELING

The discussion concentrates on the development of a cleavage-crack-initiation criterion in zinc grains. The identification is possible using a constitutive model of single-crystal zinc developed in Part I of this article^[5] and previous data on cleavage cracking in equibiaxial expansion. Model validation is then possible based on the experimental results in simple and plane-strain tension. The crystallographic aspects evidenced in Section III–C can then be explained in the last subsection of this discussion.

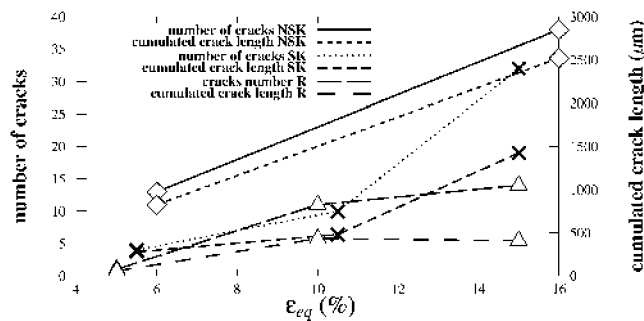


Fig. 10—Number of cracks and cumulative crack length as a function of the equivalent strain for a surface of 1 cm^2 for the three coatings strained after electropolishing (equibiaxial expansion tests).

A. Formulation of the Cleavage-Fracture Model

The driving force for cleavage-crack initiation is the stress component normal to the basal plane:

$$\sigma_n = c_i \sigma_{ij} c_j \quad [2]$$

where σ_{ij} is the stress tensor and c is the unit vector parallel to the [0001] direction. However, based on the work of Deruyttere and Greenough^[16] and Gilman,^[11] it has been shown that plastic slip on the basal plane can reduce the cleavage resistance of zinc single crystals. In these studies, it was shown that the critical normal stress leading to cleavage depends on the amount of plastic slip prior to fracture. Similar observations have been made in the case of crack propagation in textured zinc sheets.^[17] The cleavage criterion proposed by Gilman^[11] involved the product $\sigma_n \gamma_i^{\text{bas}}$, where γ_i^{bas} is the amount of slip for the basal slip system i . The corresponding cleavage-resistance curve found by Gilman for pure zinc single crystals is reproduced in Figure 11. The reason for a possible enhancement of cleavage fracture by plastic-slip activity is the existence of local stress concentrations associated with basal dislocation pileups that can locally reach the decohesion threshold for the basal plane. We will use the following expression of the critical basal normal stress (σ_n^*) for cleavage initiation:

$$\sigma_n^* = \sigma_0 + \frac{k}{\gamma_0 + \gamma_{eq}^{\text{bas}}} \quad [3]$$

where (σ_0, k, γ_0) are material parameters to be determined. The cleavage resistance in the absence of basal slip is $\sigma_0 + k/\gamma_0$. A measure of the total basal activity of all three basal slip systems is introduced:

$$\gamma_{eq}^{\text{bas}} = |\gamma_1^{\text{bas}}| + |\gamma_2^{\text{bas}}| + |\gamma_3^{\text{bas}}| \quad [4]$$

The proposed criterion states that cleavage may occur in a given grain being acted on by a given stress tensor (σ_{ij}) and currently plastically deformed by γ_{eq}^{bas} , when the basal normal stress component (σ_n) reaches the current threshold value (σ_n^*) given by Eq. [3]. Note that the form of Eq. [3] is slightly different from Gilman's original criterion. The additional parameters are intended to provide a better description of the experimental results in the identification carried out in the next section. In particular, Eq. [3] introduces an asymptotic value (σ_0) for crystals undergoing a very large amount of basal slip, which is not the case in Gilman's criterion.

B. Identification of Model Parameters from Equibiaxial Tension Tests

The parameters of the cleavage Criterion [3] have been identified from several specific expansion tests for the NSK coating. For that purpose, the stress and plastic states of a given zinc grain are estimated using the relaxed-constraint Taylor model developed in Part I of this article.^[5] The main features of the model are now recalled. For given loading conditions prescribed to the coated steel sheet (tension, plane-strain tension, and equibiaxial expansion), the in-plane strain components ϵ_{11} , ϵ_{22} , and ϵ_{12} that the substrate is subjected to are computed using an anisotropic Hill plasticity model. These computed strain components are then imposed to a zinc single crystal having a given crystal orientation. The

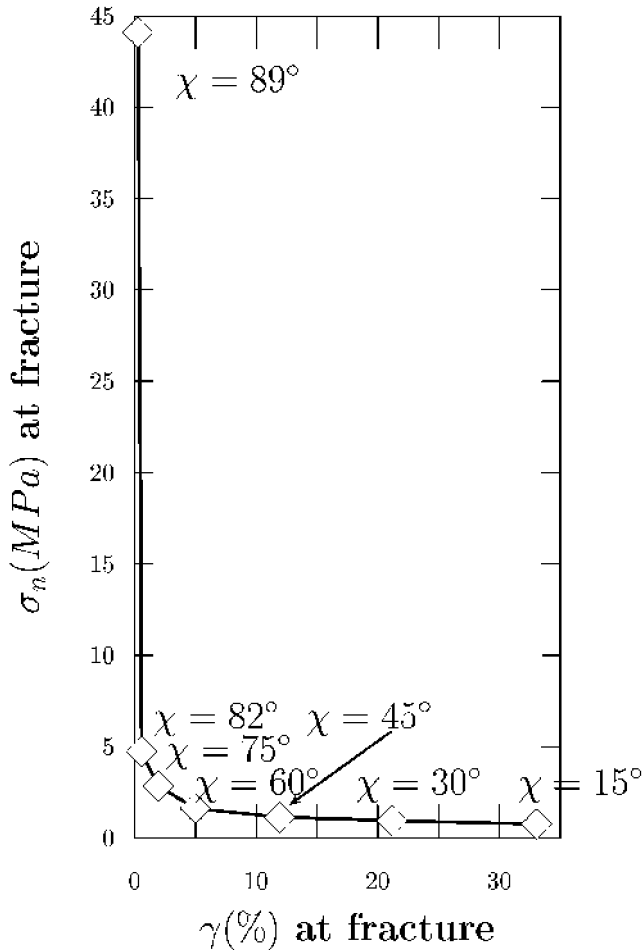


Fig. 11—Normal stress to the basal plane, at fracture, as a function of basal glide for different misorientations χ between the c -axis and the tensile direction.^[16,11]

vanishing-stress components σ_{33} , σ_{13} , and σ_{23} are also prescribed to this grain. The stress and strain states are assumed to be homogeneous in the grain. This crude approximation has been validated by finite-element computations in Reference 15. The resulting stress components (σ_{11} , σ_{22} , and σ_{12}) are deduced using the constitutive single-crystal model identified in References 15 and 5.

Four samples of the NSK galvanized steel sheet have been thus tested, respectively, at 3, 5, 7, and 10 pct equivalent strain. These tests have been performed specifically for the identification of the cleavage criterion, so that they have not been reported in Section III. Note that this is not a single test interrupted 4 times, but these are four distinct specimens. Therefore, the analysis of cleavage cracking must be carried out over a sufficient number of grains. After each expansion test, the cleavage cracks on a surface of 1 cm² are counted in each sample. The orientations of all observed damaged grains are determined using the EBSD technique. As expected from the quantitative analysis of Section III-D, the number of observed damaged grains on a 1 cm² surface increases for increasing overall deformation.

The relaxed-constraint Taylor model can now be applied to these different grains and at four different overall strain

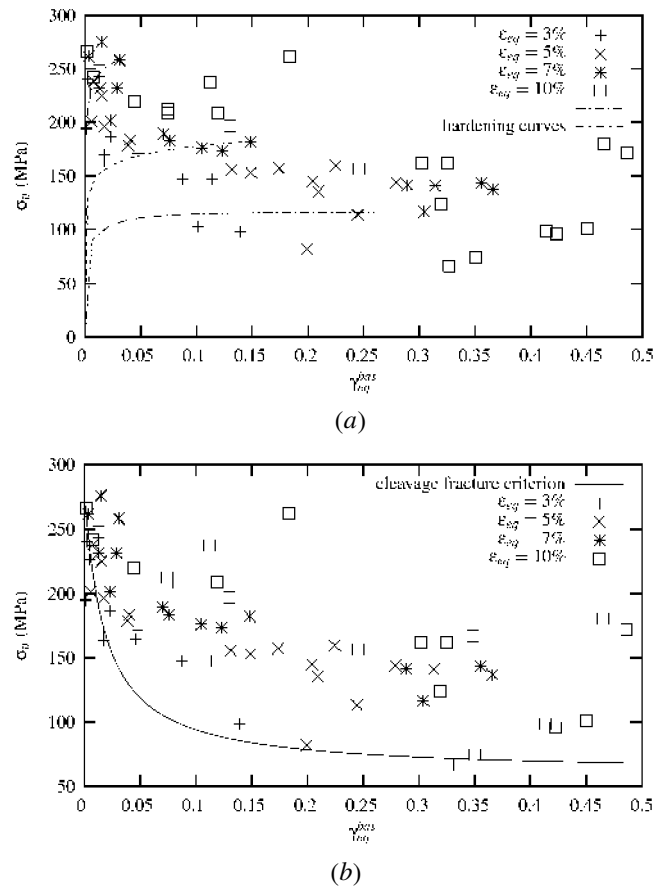


Fig. 12—Normal stress to basal plane vs equivalent plastic strain due to basal slip for grains containing cleavage cracks, at various overall equivalent strain levels (equibiaxial expansion tests). (a) The hardening curves of three grains of the specimen tested up to 7 pct. (b) The cleavage fracture criterion is superimposed to the points.

levels. It is then possible to plot the computed basal normal stress (σ_n) vs the measure of total slip activity (γ_{eq}^{bas}) for all damaged grains observed at the four different overall strain levels. The results are shown in Figure 12(a). Three full loading curves are shown in Figure 12(a) as examples of the performed computations. The final state only is plotted for the other grains. Note that all grains considered in Figure 12 display cleavage cracks, according to the experimental observations. This means that the computed component σ_n must exceed the postulated threshold σ_n^* . These computed values provide an estimation of the threshold value. However, this is only an upper bound for a given overall strain level. The cleavage cracks observed in a grain of a sample deformed up to 7 pct, for instance, may have occurred at any strain level between 5 and 7 pct. That is why the cleavage-threshold curve is defined as the lower envelope of the σ_n vs γ_{eq}^{bas} cloud of points in Figure 12. It means that only the points with the lowest normal stress values are assumed to be close to the σ_n^* value corresponding to the overall equivalent strain level at which they are observed. The obtained estimation of the threshold curve is shown in Figure 12(b). The resulting material parameters giving the best fit for this estimation of the cleavage-threshold curve are given as follows:

$$\sigma_0 = 60 \text{ MPa}, \quad k = 4 \text{ MPa}, \quad \gamma_0 = 0.018 \quad [5]$$

We observe a drastic decrease of the critical normal stress for cleavage at increasing basal plastic deformation, which is less pronounced, however, than that for Gilman's curve of Figure 11 for pure zinc single crystals. The ratio of the critical normal stress values at 0 and 0.1 basal plastic slip is found to be 20 for Gilman's curve and only 3 in our case (compare the curves of Figures 11 and 12(b)). Note that both curves have been identified for very different loading conditions. Gilman has collected the results of tensile tests on single crystals, whereas the grains studied here are subjected to strongly multiaxial loading conditions (equibiaxial expansion tests). Furthermore, our identification procedure gives a poor description of the cleavage threshold in the domain of the curve for which γ_{eq}^{bas} is close to zero. This may lead to an underestimation of the cleavage threshold at $\gamma_{eq}^{bas} = 0$, which is very high in Gilman's curve. It can also be seen that the considered coating is considerably harder than pure zinc, due to the content of alloying elements. This has been discussed in Reference 18 regarding the tensile behavior.

Although the proposed criterion may still be valid, the previous analysis cannot be performed for the two other microstructures. The reason is that the relaxed-constraint Taylor model is valid only for flat pancake grains and collapses for finer microstructures, as proven in Part I of this article in the case of the recrystallized coating. In the latter case, a full finite-element analysis of a set of zinc grains on the substrate is necessary, since the stress/strain fields become very heterogeneous from the interface to the free surface and even laterally (Figure 16 in Reference 5). The cleavage criterion should then be applied locally at all integration points within each grain. This was out of the scope of the present study.

C. Application to Other Loading Conditions

The aforementioned cleavage-fracture model identified from equibiaxial expansion tests is now applied to the other loading conditions considered in this work, namely, simple tension and plane-strain tension. For that purpose, the following procedure is retained. The orientations of 15 grains are considered that have been damaged during an equibiaxial expansion test after $\varepsilon_{eq} = 3$ pct. The responses of the same grains are now simulated when they are subjected to plane-strain tension and simple tension. The computed basal normal stress component and total basal slip are plotted in Figure 13. They are compared to the cleavage-fracture curve. Points below the cleavage threshold will not be damaged. Cleavage cracks are expected to occur in the grains corresponding to points above the failure criterion.

It appears that no damage is expected in pure tension. This is in accordance with the experimental observations in tensile specimens for the NSK coating. Two or three grains close to the failure curve are expected to be damaged during a plane-strain tension test. This is about 3 times less than for an equibiaxial tension test. This result is to be compared to the ratio of the number of cracks for both loading conditions found in Figure 9(a). This confirms the experimental observations made in Section III-B, showing that the plane-strain test is significantly less damaging than the equibiaxial expansion test.

The simulation of many other orientations would be necessary to confirm this first validation procedure. Comparison

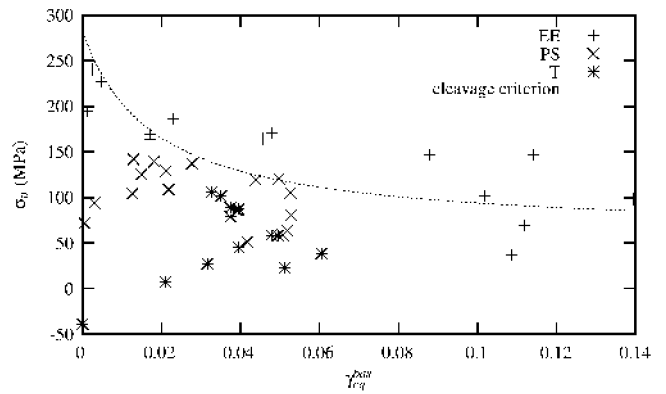


Fig. 13—Comparison of the predicted response of 15 grains having the orientations of damaged grains in the specimen tested after 3 pct equivalent deformation in equibiaxial expansion test: tension, plane strain, and expansion tests. The limit curve corresponding to the cleavage criterion is also represented, showing that, for the same equivalent strain, tensile straining is less damaging than expansion (EE, PS, and T stand for equibiaxial expansion, plane strain tension, and simple tension, respectively).

carried out for tests at larger strain levels than $\varepsilon_{eq} = 3$ pct are also satisfactory, although with growing discrepancy for increasing strain.

D. Crystallographic Aspects

Another validation of the proposed cleavage model is possible by looking at the preferred orientations of damaged grains. This is done now in the case of the NSK coating subjected to plane-strain tension in the RD. For cleavage to occur, the normal stress component must be high enough. It is maximal for grains having their c -axis along the tensile RD. However, for such ideal orientations, the cleavage threshold is very high. A slight misorientation from this ideal orientation leads to a significant decrease of the threshold due to the early activation of basal slip, according to Formula [3]. For misorientations larger than about 30 deg, the basal normal stress becomes too small and cleavage cannot occur. This is in accordance with the observed orientations of damaged grains during a plane-strain test represented by the pole figures of Figures 8(a) and (b) on the left-hand side.

Is it possible now to explain the pole figures in Figures 8(a) and (b) on the right-hand side, showing that the $\langle 10\bar{1}0 \rangle$ direction of damaged grains lies preferentially along the ND of the sheet. This can, in fact, be proven to be due to the preferential simultaneous activation of several basal slip systems. For that purpose, let us consider the two following ideal grain orientations described by their Euler angles:

1. Orientation 1: ($\phi_1 = 90$ deg, $\Phi = 90$ deg, $\phi_2 = 90$ deg)
2. Orientation 2: ($\phi_1 = 90$ deg, $\Phi = 90$ deg, $\phi_2 = 0$ deg)

The angles are given with respect to the frame (RD, TD, ND) of the steel sheet. The c -axis of both grains coincides with the RD. The direction $[10\bar{1}0]$ corresponding to the orientation 2 coincides with the ND of the sheet, whereas it lies 30 deg away from ND for orientation 1. Grains having these ideal orientations and subjected to plane-strain tension

will not undergo any basal slip. Let us slightly perturb these orientations, for instance, by a small angle α :

1. Orientation 1: ($\phi_1 = 90 \text{ deg} - \alpha$, $\Phi = 90 \text{ deg}$, $\phi_2 = 90 \text{ deg} + \alpha$)
2. Orientation 2: ($\phi_1 = 90 \text{ deg} - \alpha$, $\Phi = 90 \text{ deg}$, $\phi_2 = \alpha$)

The pole figures corresponding to both orientations in the special case $\alpha = 4 \text{ deg}$ are shown in Figure 14 as an example. The grains with the general perturbed orientation α are now subjected to a biaxial stress tensor with two nonvanishing components, σ_1 and σ_2 , corresponding to the components σ_{11} and σ_{22} in the frame of the sheet. The corresponding resolved shear stresses on the three basal slip systems are now computed for both general perturbed orientations. The basal slip systems are called Be, Bf, and Bg in the classification proposed in Reference 19 and have been recalled in Table I of Part I of this article. They are labeled 1, 2, and 3, respectively, in the following equations:

$$\tau_1^1 = \frac{1}{2} \sin \alpha \cos \alpha (\sigma_1 - \sigma_2) (\sqrt{3} \cos \alpha + \sin \alpha) \quad [6]$$

$$\tau_2^1 = \sin^2 \alpha \cos \alpha (\sigma_2 - \sigma_1) \quad [7]$$

$$\tau_3^1 = \frac{1}{2} \sin \alpha \cos \alpha (\sigma_1 - \sigma_2) (\sqrt{3} \cos \alpha - \sin \alpha) \quad [8]$$

$$\tau_1^2 = \frac{1}{2} \sin \alpha \cos \alpha (\sigma_1 - \sigma_2) (\cos \alpha - \sqrt{3} \sin \alpha) \quad [9]$$

$$\tau_2^2 = \sin \alpha \cos^2 \alpha (\sigma_2 - \sigma_1) \quad [10]$$

$$\tau_3^2 = \frac{1}{2} \sin \alpha \cos \alpha (\sigma_2 - \sigma_1) (\cos \alpha + \sqrt{3} \sin \alpha) \quad [11]$$

The superscript refers to the grain orientation and the subscript to the slip-system number. All resolved shear stresses vanish

for $\alpha = 0$. The absolute values of these resolved shear stresses increase for increasing $|\alpha|$ values. The only qualitative difference between these resolved shear stresses is that all start from $\alpha = 0$ with a nonzero tangent, except τ_2^1 . This means that a slight misorientation from the ideal orientation 1 will not significantly change the activity of slip system 2, whereas all other slip systems will be triggered. The main consequence is that γ_{eq}^{bas} will be greater for perturbed orientation 2 than for orientation 1. This is confirmed by a numerical simulation for $\alpha = 4 \text{ deg}$ for instance, which predicts almost 10 times more total basal slip for orientation 2 than for orientation 1. Accordingly, grains close to orientation 2 are more prone to cleavage, according to Criterion [3]. This is in accordance with the experimental observation of cleavage cracks in grains close to orientation 2 rather than to orientation 1.

The observed preferential orientations of damaged grains with respect to the loading axes must be confirmed by investigating the response of grains having orientations different from the previous orientations 1 and 2. Two examples are provided as follows. First, an isotropic distribution of 1000 grains with random orientations is considered. Each grain is subjected to a plane-strain tensile test in the RD and its response is simulated using the relaxed-constraint Taylor model. The cleavage-fracture criterion is evaluated after 10 pct equivalent straining for each grain. The results are illustrated by the pole figures of Figure 15: grains fulfilling the cleavage conditions are represented by larger dark spots, the size of which is proportional to the difference between the basal normal stress and the cleavage threshold. The undamaged grains are not represented. The $[0002]$ and $\langle 10\bar{1}0 \rangle$ pole figures are found to be in good agreement with the experimental ones (Figure 8). Second, the same simulations have been performed using 9000 orientations respecting the actual texture of the NSK coating. The results are very similar to those found using an isotropic distribution. This confirms that the texture does not introduce a bias in the observed preferential orientations of cleaved grains. The texture affects, of course, the number of damageable grains.

V. CONCLUSIONS

Zinc coatings of the investigated hot-dip galvanized steel sheets exhibit an exceptional resistance to spalling due to several deformation and local damage mechanisms. No evidence of interfacial coating/substrate damage was found in any investigated material after all the tests. All the coatings display a formidable capacity of accommodating the deformation activated by the substrate and of relaxing the induced highly multiaxial stresses. The relaxation mechanisms evidenced in this work are the following.

1. Several slip-system families are successively activated for increasing stress levels, depending on the grain orientation: basal, pyramidal π_2 , or prismatic slip.^[5]
2. Deformation twins can form regular networks. They reduce the stress concentrations at cleavage-crack tips. Configurations showing twins left behind the crack tip have been observed.
3. Grain-boundary cracking occurs very early during the deformation of the coating, but it has been shown that the cracks do not reach the substrate. Intergranular cracking leads to a relaxation of higher stresses at grain boundaries due to plastic incompatibilities, especially for the NSK coating.

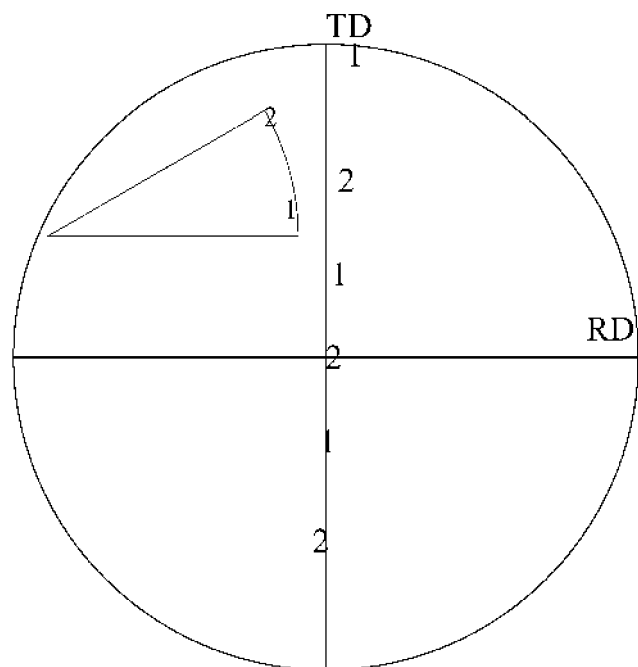


Fig. 14—Inverse and $\langle 10\bar{1}0 \rangle$ -direct pole figures showing two typical grain orientations that can lead to cleavage under plane strain tension in direction RD.

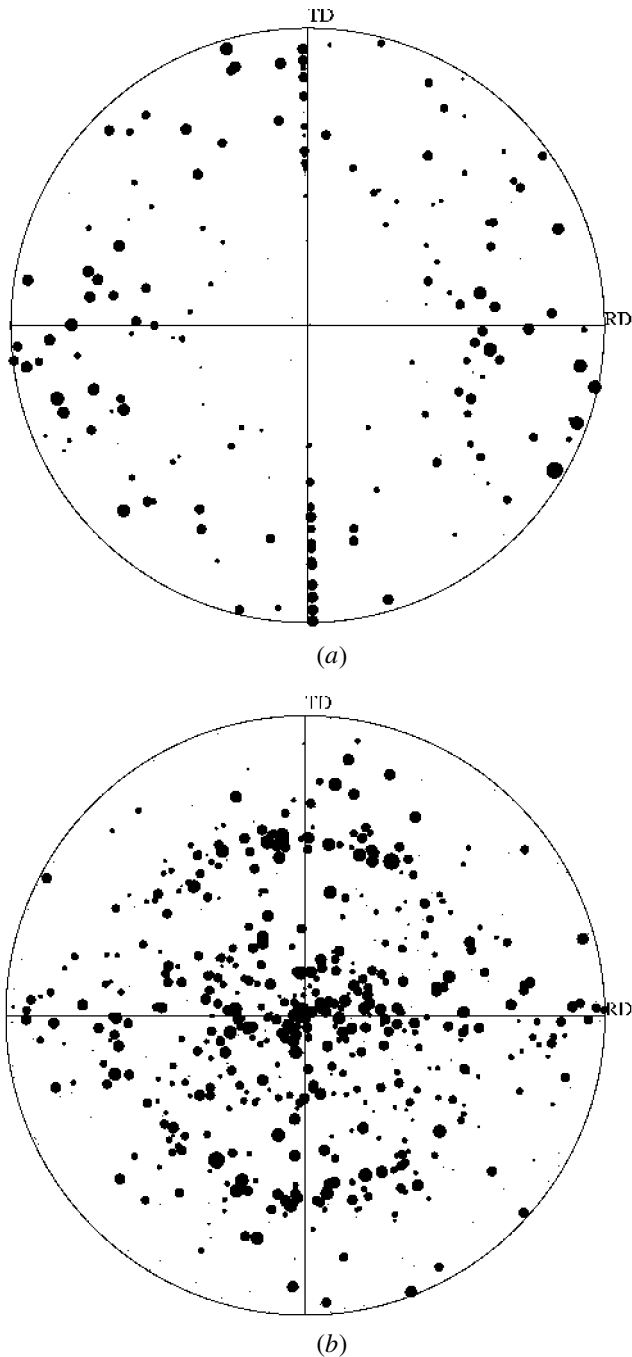


Fig. 15—(a) and (b) Pole figures representing cleaved grains according to the numerical simulation: (0002) pole figure on the left and $\langle 10\bar{1}0 \rangle$ pole figure on the right. A plane strain test has been simulated using the relaxed constraint Taylor model up to 10 pct for 1000 random initial grain orientations. The radius of each spot is proportional to the difference between the stress amount in direction c and the cleavage threshold (Eq. [3]).

4. Cleavage cracks occur only in the case of highly multiaxial conditions met during plane-strain tension and equibiaxial expansion tests. They have been shown to reach the coating/substrate interface, but they do not open further. Instead, they multiply, forming parallel crack networks in several grains.

These properties of zinc coatings can even be improved by specific deformation or heat treatments. A slight tempered

rolling introduces many small twins that are efficient obstacles to cleavage-crack propagation, as shown in this work for the SK coating. Grain refinement by recrystallization heat treatment also leads to an improved resistance of the coating to cracking, as shown for the recrystallized coating. Drastic reductions of the number and length of cracks have been obtained and measured quantitatively for these two coatings in comparison to the NSK material. This must be related also to the fact that accommodation of the deformation prescribed by the substrate to the coating at the interface leads to a strain gradient from the interface to the free surface in the case of small grains, as evidenced in Part I of this article.

The relaxed-constraint Taylor model combined with an adequate cleavage-fracture criterion has been shown to be appropriate for the prediction of damage in the pancake grains of the NSK coating. It correctly accounts for the hierarchy of performed tests: tension is less damaging than plane-strain tension, equibiaxial expansion being the most severe loading condition. The crystallographic features of the coating deformation under plane-strain conditions are also correctly described by the model. The influence of basal slip activity on cleavage fracture, once evidenced by Gilman for a pure zinc single crystal, also plays a major role in the damage of zinc coatings with flat grains.

Several aspects of the modeling approach must be improved. First, the relaxed-constraint Taylor model has been used in its small-strain formulation for simplicity. It can readily be extended to incorporate possible lattice rotations. The simulation of deformation twinning and its interaction with plasticity is a major difficulty to be overcome for a better understanding of local deformation mechanisms like the observed development of twin networks. First steps in this direction have been presented in Reference 20.

REFERENCES

1. S. Lazik, C. Esling, and J. Wegrial: *Text. Microstr.*, 1996, vol. 23, pp. 131-47.
2. J. Lietzau, M.J. Philippe, C. Esling, J. Wegria, and M. Dubois: in *Zinc-Based Steel Coating Systems*, F.E. Goodwin, ed., TMS, Warrendale, PA, 1998, pp. 207-17.
3. S.R. Shah, J.A. Dilewijns, and R.D. Jones: *J. Mater. Eng. Performance*, 1996, vol. 5, pp. 601-08.
4. J.W. Christian: *The Theory of Transformation in Metals and Alloys*, Pergamon Press, Elmsford, NJ, 1965.
5. R. Parisot, S. Forest, A. Pineau, F. Grillon, X. Démonet, and J.-M. Mategne: *Metall. Mater. Trans. A*, 2004, vol. 35A, pp. 797-811.
6. H. Conrad and J. Narayan: *Acta Mater.*, 2002, vol. 50, pp. 5067-78.
7. C. Maeda, J. Shimomura, H. Fujisawa, and M. Konishi: *Scripta Metall.*, 1996, vol. 35, pp. 333-38, 1996.
8. J. Foct: *Scripta Metall. Mater.*, 1993, vol. 28, pp. 127-32.
9. Y. Leprêtre, J.-M. Mategne, M. Guttman, and J. Philibert: in *Zinc-Based Steel Coating Systems*, F.E. Goodwin, ed., TMS, Warrendale, PA, 1998, pp. 95-106.
10. G. Reumont, J.B. Vogt, A. Iost, and J. Foct: *Surface Coatings Technol.*, 2001, vol. 139, pp. 265-71.
11. J.J. Gilman: *Trans. TMS-AIME*, 1958, vol. 200, pp. 783-91.
12. A.R. Marder: *Progr. Mater. Sci.*, 2000, vol. 45, pp. 191-271.
13. B.A. Bilby and R. Bullough: *Phil. Mag.*, 1953, vol. 45, pp. 631-46.
14. M.H. Yoo: *Metall. Trans. A*, 1981, vol. 12A, pp. 409-18.
15. R. Parisot, S. Forest, A.-F. Gourgues, A. Pineau, and D. Mareuse: *Comput. Mater. Sci.*, 2001, vol. 19, pp. 189-204.
16. A. Deruyttere and G.B. Greenough: *J. Inst. Met.*, 1956, vol. 84, p. 337.
17. F. Lemant and A. Pineau: *Eng. Fract. Mech.*, 1981, vol. 14, pp. 91-105.
18. F. Barbe, R. Parisot, S. Forest, and G. Cailletaud: *J. Phys. IV*, 2001, vol. 11, pp. Pr5-277-Pr5-284.
19. C. Tomé and U.F. Kocks: *Acta Mater.*, 1985, vol. 33, pp. 603-21.
20. S. Forest and R. Parisot: *Rendiconti del Seminario Matematico dell'Università e del Politecnico di Torino*, 2000, vol. 58, pp. 99-111.